

# Enhanced Thermal Stability of Aerosol-Synthesized Ni-Rich Li-Ion Battery Cathode Materials via Concentration-Gradient Ca Doping

Ying Lin, Christopher M. Abram, Xuan Shi, Ian G. McKendry, Ziyu Wang, Hongtao Zhong, Hao Zhao, Xiaofang Yang, Bruce E. Koel, Chao Yan,\* and Yiguang Ju



Cite This: *ACS Appl. Energy Mater.* 2022, 5, 10751–10757



Read Online

ACCESS |

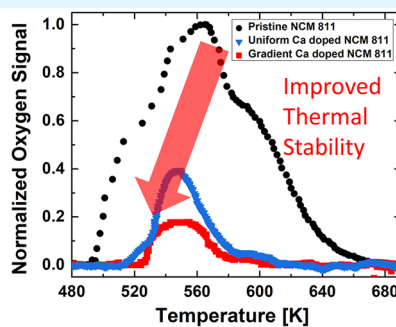
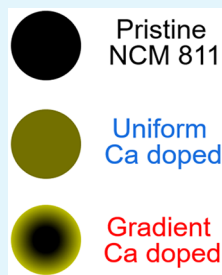
Metrics & More

Article Recommendations

Supporting Information

**ABSTRACT:** High-Ni cathode materials such as  $\text{LiNi}_{0.8}\text{Co}_{0.1}\text{Mn}_{0.1}\text{O}_2$  (NCM811) are replacing low-Ni, high-Co cathode materials in Li-ion batteries. However, the poor thermal stability and long-term cycling performance of high-Ni cathode materials are a barrier to rapid commercial application. Doping is used to optimize the fire safety and electrochemical performance of NCM811. In this work, we synthesized calcium (Ca)-doped NCM811 materials with direct control of the local dopant concentration by using an aerosol synthesis process (rapid metal salt solution aerosol pyrolysis). By identifying the appropriate precursors and controlling the ion concentrations and precursor solubility in solution, we have shown that both a uniform dopant concentration and a unique gradient structure of Ca can be controllably formed within the NCM811 cathode particles. This Ca-doping technique significantly increased the thermal stability of NCM811. In thermal decomposition tests of the delithiated materials, the oxygen release of uniform and gradient Ca-doped NCM811 decreased by 52 and 85%, respectively, as compared to that of the undoped materials. Furthermore, the thermal onset temperature was increased from 498 to 527 K. Herein, we show that rapid formation of a concentration-gradient structure in aerosol synthesis is a promising route to optimize the thermal stability of cathode materials for Li-ion batteries.

**KEYWORDS:** *Li-ion batteries, thermal stability, calcium doping, gradient structure, Ni-rich cathode materials*



## 1. INTRODUCTION

Nowadays, lithium-ion batteries (LIBs) are key energy devices widely used in portable electronics, power tools, transportation, and energy storage.<sup>1,2</sup> Increasing research focus is on Ni-rich cathode materials to achieve a higher energy density,<sup>3–6</sup> with Ni-rich ternary cathode materials such as  $\text{LiNi}_{0.8}\text{Co}_{0.1}\text{Mn}_{0.1}\text{O}_2$  (NCM811) garnering particular interest due to the high energy and power density.<sup>7</sup> However, safety issues due to the increased nickel concentration still present major hurdles, limiting its further commercialization due to the presence of highly reactive  $\text{Ni}^{3+/4+}$ .<sup>7</sup> Decomposition of cathode materials at elevated temperatures with subsequent exothermic oxygen release can result in battery combustion.

Battery fires are a cause of high safety concern because of their high intensity and long duration due to thermal runaway. It happens in three successive processes.<sup>8</sup> In stage 1, battery operation becomes abnormal, which could be triggered by external overheating, short-circuiting, or overcharging. When the battery's internal temperature goes beyond a critical point, the battery reaches stage 2, where the battery internal temperature quickly rises and releases flammable gases, hydrocarbons, and oxygen by decomposition of the solid electrolyte interphase, anode, and cathode, respectively.<sup>9</sup> Solid

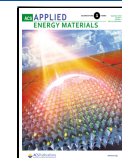
electrolyte interphase decomposition, lithium metal reaction, and cathode breakdown are the major contributors at this stage, and importantly all three ingredients in the combustion triangle (i.e., heat, fuel, and oxidizer) are provided. For NCM LIBs, the high-nickel formulations increase the amount of unstable  $\text{Ni}^{4+}$ , which induces fast reduction reactions during thermal decomposition. In contrast, Mn and Co improve the thermal stability but are present in lower concentrations in NCM811 material.<sup>10</sup> After oxygen release from cathode material decomposition, battery combustion and explosion initiate in stage 3.

To prevent thermal degradation of the cathode materials, coating is a widely applied technique in the battery industry.<sup>11,12</sup> It shields the cathode materials from direct contact with the electrolyte by forming an interface and alleviates the reactions between cathode material and electro-

Received: May 13, 2022

Accepted: August 8, 2022

Published: August 22, 2022



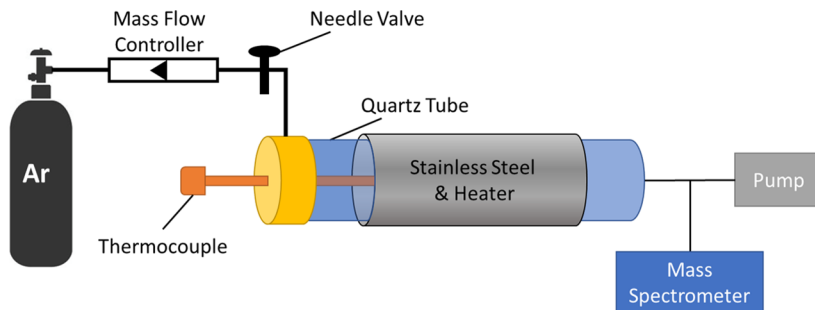


**Figure 1.** Schematic drawing of the thermal decomposition micro-flow reactor.

lyte.<sup>13</sup> Metal oxides such as  $\text{Al}_2\text{O}_3$ ,  $\text{B}_2\text{O}_3$ ,  $\text{ZrO}_2$ , and  $\text{TiO}_2$  are commonly used as the coating material due to their high chemical stability limiting the interaction of unstable  $\text{Ni}^{4+}$  with organic electrolyte solvents.<sup>14–17</sup> However, there are some drawbacks of the surface coating approach. Primarily, the coating process of cathode material induces additional processing steps and cost for cathode manufacturing. Additionally, metal oxide coatings can reduce electrical conductivity, alter the cathode material crystal structure, and impair long-term thermal stability due to non-uniformity of the coating.<sup>18</sup>

Doping is another promising strategy for improving Ni-rich cathode safety. Wang et al.<sup>19</sup> demonstrated that yttrium surface gradient doping could improve battery thermal stability. Calcium is a promising dopant since it can stabilize the Ni oxide lattice structure and improve the electrochemical performance of LIBs.<sup>20,21</sup> In high-Ni cathode material, cation mixing due to the similar radii of  $\text{Li}^+$  and  $\text{Ni}^{2+}$  is one of the major factors that limit the cyclability due to the reduced  $\text{Li}^+$  diffusion in the charge–discharge process.<sup>22,23</sup> Previous studies showed that doping elements with a large ionic radius help stabilize the layered structure.<sup>24</sup> Calcium has the largest radius (0.1 nm) among the abundant divalent metals, which makes it a perfect doping element. We hypothesized that Ca doping can have additional positive effects with regard to thermal runaway. Ni cations are present as high-valence  $\text{Ni}^{4+}$  after charging, but during the thermal decomposition process,  $\text{Ni}^{4+}$  is reduced to the low-valence  $\text{Ni}^{2+}$  and releases oxygen.<sup>10</sup> A good example is delithiated  $\text{Li}_x\text{NiO}_2$ , where  $\text{Ni}^{2+}$  is unstable in the layered crystal structure. The ionic size similarity between  $\text{Ni}^{2+}$  and  $\text{Li}^+$  tends to convert less stable  $\text{Li}_x\text{NiO}_2$  to more stable  $\text{LiNi}_2\text{O}_4$ , oxygen, and  $\text{NiO}$ .<sup>8,25,26</sup> Due to the higher reactivity of Ca compared to Ni, Ca tends to react with oxygen before Ni, so that Ca doping can localize lattice oxygen, decelerate the reduction process, and change the reaction pathway to produce solid products. In summary, by developing a novel Ca doping method, Ni-rich cathode materials may offer improved safety while maintaining high performance.

Herein, we show that enhanced thermal stability in NCM811 Ni-rich cathodes was achieved by a novel Ca doping technique, requiring no further coating processes. Ca is successfully doped into NCM811 cathode material in both targeted gradient and uniform distributions at controlled doping concentrations of 1.5% using high-temperature aerosol synthesis, thereby rapidly and controllably incorporating the Ca dopant throughout the material or on the particle surface to stabilize the structure and the cathode–electrolyte interface, respectively. The unique Ca-doped NCM811 materials are compared to undoped pristine NCM811 and are shown to noticeably enhance the thermal/chemical stability, where the

temperature onset of  $\text{O}_2$  release is increased and the overall amount of  $\text{O}_2$  evolution is reduced.

## 2. METHODS

The Ni-rich cathode material particles were synthesized from a precursor solution that consisted of Ni, Co, Mn, and Li nitrates dissolved in distilled water.  $\text{Ni}(\text{NO}_3)_2 \cdot 6\text{H}_2\text{O}$ ,  $\text{Co}(\text{NO}_3)_2 \cdot 6\text{H}_2\text{O}$ , and  $\text{Mn}(\text{NO}_3)_2 \cdot 4\text{H}_2\text{O}$  were weighed to achieve a molar ratio of 8:1:1 with a total concentration of 1 mol/L solution. 1.05 mol of Li nitrate and 0.015 mol of calcium salts (1.5% molar ratio to NCM material) were then added. For the precursor to produce a uniform structure material, 0.015 mol of calcium nitrate was used for Ca doping (uniform 1.5% Ca-doped NCM811). For the gradient structure material, 0.0075 mol of calcium oxide dissolved in 1 mol/L sulfuric acid and 0.0075 mol of calcium nitrate added into the precursor solution (gradient 1.5% Ca-doped NCM811) were used for Ca doping. Such differences in the Ca doping precursor solutions were designed for controlled evaporation and precipitation processes with vastly different solubility values of the Ca salts.

The materials were synthesized by a high-temperature aerosol method with a custom reactor. The method and reactor have been introduced in detail in our previous report.<sup>27</sup> The aerosol synthesis approach requires two steps for synthesizing the cathode materials: (1) formation of solid particles and (2) sintering in an  $\text{O}_2$  atmosphere.<sup>28</sup> In the first step, the precursor solution underwent atomization using a 1.7 MHz ultrasonic transducer array. 3–5  $\mu\text{m}$ -diameter precursor droplets were generated using an atomizer and then flowed through the preheating zone and bulk heating furnace. In the three-stage preheating ( $100^\circ\text{C}$ ,  $140^\circ\text{C}$ , and  $180^\circ\text{C}$ ), the precursor droplet slowly evaporated to an anhydrous droplet. After the preheating stage, the droplet went through bulk heating ( $800^\circ\text{C}$ ) in a tube furnace; this section decomposed the precursor material that forms the product powder. Product powder was collected with filter paper and a vacuum pump. By controlling the evaporation rate and preheating/bulk temperature, the morphology and size of the synthesized particles can be controlled. During the synthesis process, cathode material particles were formed during the droplet evaporation process instead of the traditionally applied coprecipitation method—growing from the nucleation and precipitation in solution. It is possible to modify the synthesis process and to form non-equilibrium material with the aerosol method. The morphology is strongly affected by the ratio of the solvent evaporation time to solute diffusion time ( $\tau_{\text{evap}}/\tau_{\text{diff}}$ ). Moreover, the calcium sulfate precursor solubility in water (2.6 g/L) is significantly lower than calcium nitrate solubility (1212 g/L). Calcium sulfate precipitated earlier than other elements with water evaporation from the droplet, forming a Ca-rich surface. In contrast, the solubility of all elements is not largely different from that of calcium nitrate, so in the other case, calcium precipitated homogeneously with the other elements and generated a uniform Ca-doped structure. After the first step, product powders were annealed in a tube furnace at  $800^\circ\text{C}$  with a constant oxygen flow (0.5 LPM) for 12 h to improve the crystallinity, form a layered structure, and reduce the ion mixing of NCM811.

The synthesized Ni-rich cathode product powders were characterized before and after annealing. They were imaged by high-

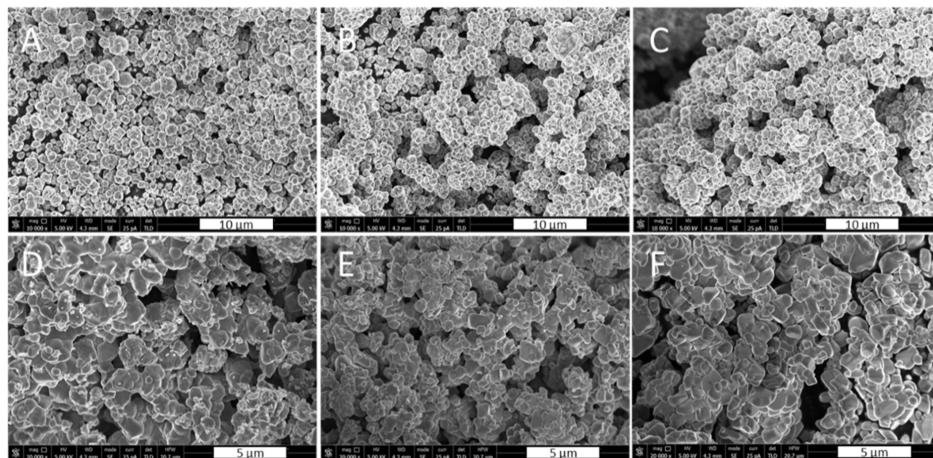


**Figure 2.** SEM images of precursors and annealed cathode materials: (A) pristine NCM811 precursor, (B) uniform 1.5% Ca-doped NCM811 precursor, (C) gradient 1.5% Ca-doped NCM811 precursor, (D) pristine NCM811-800 °C, (E) uniform 1.5% Ca-doped NCM811-800 °C, and (F) gradient 1.5% Ca-doped NCM811-800 °C.

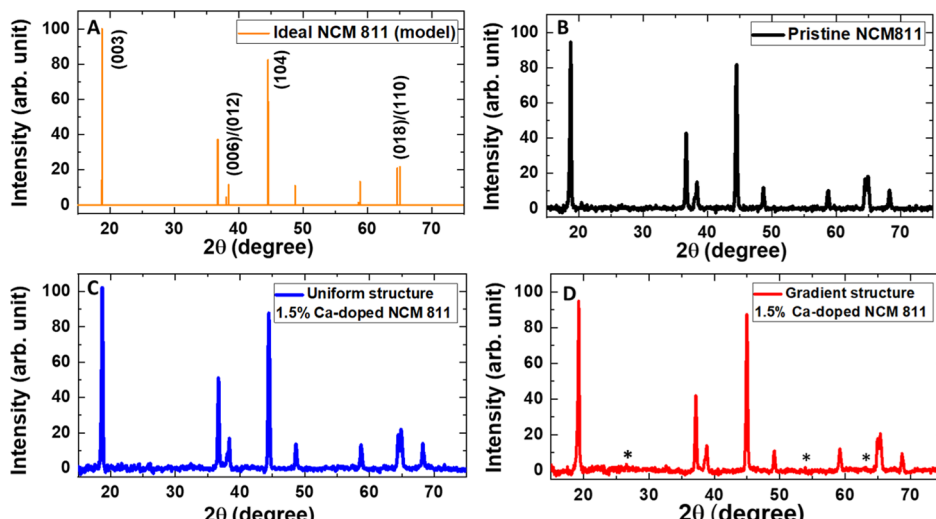


**Figure 3.** XRD results for (A) XRD model of ideal NCM811 and (B) XRD of pristine NCM811, (C) uniform Ca-doped material, and (D) gradient Ca-doped material.

resolution scanning electron microscopy (HR-SEM) (Quanta 200 FEG Environmental SEM, FEI) for particle size and morphology, characterized by elemental analysis using energy-dispersive X-ray spectroscopy (EDX) (Oxford Instruments) built into HR-SEM, probed by X-ray powder diffraction (XRD) (D8 Discover, Bruker, Cu K- $\alpha$  X-ray) for the crystal structure, and analyzed for surface chemical composition by high-resolution X-ray photoelectron spectroscopy (HR-XPS) (K-Alpha, Thermo Fisher) in a region 400 nm  $\times$  400 nm. Argon-ion etching using a cluster ion source was used to obtain the depth profile of the material. In this report, the etching time was up to 1200 s, and the ion energy was 3500 eV.

The cathode samples were also assembled in CR-2032 coin-type full cells to determine the electrochemical properties. Electrochemical testing was performed using a battery testing system (CT-3008, Neware) between 2.8 and 4.3 V for the potential window. The active materials were assumed to have a discharge capacity of 200 mA h/g. In the first cycle, the cells were charged by the constant-current/constant-voltage (CCCV) method at C/10 with a cutoff current of C/50 and then discharged by the constant-current (CC) method at a C/10 rate.

Furthermore, as a key feature of battery safety, we tested the thermal/chemical stability of the cathode materials. Thermal decomposition tests were conducted in a micro-flow reactor. The reactor was made by using a 1/4 in.-diameter quartz tube and heating

element loaded with a coaxial stainless-steel tube in the reaction zone as shown in Figure 1. A thermocouple was inserted into the reaction zone to monitor the temperature. In the reactor exhaust, the gaseous products were analyzed using a mass spectrometer. Cathode materials were charged in a “large cell” to 4.3 V. The large cell is a scale-up CR-2032 coin-type full cell that has a 2.5 cm diameter. The large cell is installed and charged in exactly the same way as a typical CR-2032 coin-type cell. Such a large cell provides enough consistent material for thermal/chemical stability tests. After charging, the cell was disassembled in an Ar-filled glovebox, and the delithiated cathode material was washed with diethylene carbonate. 200 mg of material was weighed and loaded into a reactor. Helium was used as the purge gas and continuously fed at 50 mL/min into the reactor during experiments. During a thermal decomposition test, the reactor was linearly heated from 400 to 800 K with a heating rate of 5 K/min. The heating rate and temperature region were calibrated by a reference heating test using only heated purge gas without cathode material. The reference heating test also proved that the temperature effect from material loading is ignorable.

### 3. RESULTS AND DISCUSSION

As shown in Figure 2A–C, all three precursors for the cathode materials [i.e., pristine NCM811 (A), uniform Ca-doped

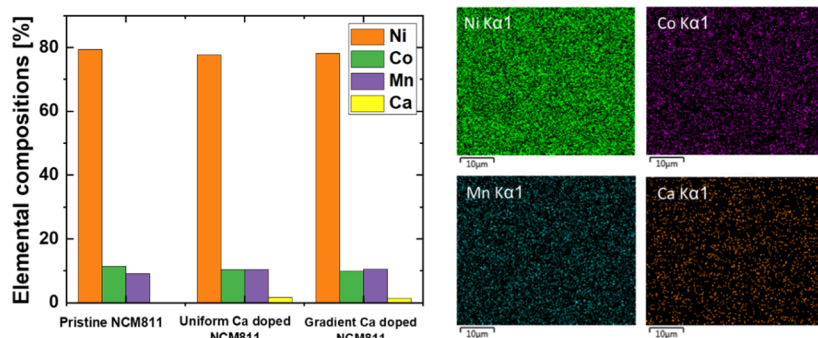


**Figure 4.** Left: EDX elemental concentrations of NCM811 materials. Right: EDX mapping images.

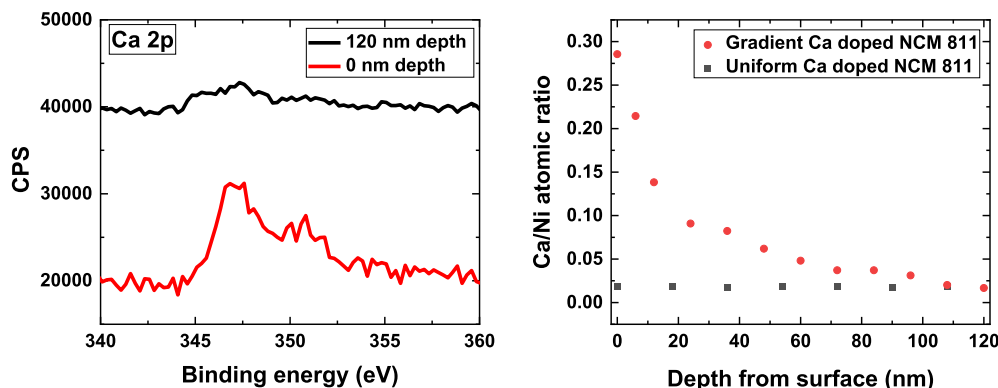


**Figure 5.** Left: XPS Ca2p region scans for gradient Ca-doped NCM811 for 0 nm depth (red) and 120 nm depth (black). Right: Ca concentration decreases with depth, confirming a gradient structure in the material using a calcium sulfate precursor. Gradient Ca-doped NCM811 (red) and uniform Ca-doped NCM811 (black).

NCM811 (B), and gradient Ca-doped NCM811 (C)] were imaged by SEM and confirmed to possess similar particle sizes and spherical morphologies. The particle sizes range from 0.2 to 2.1  $\mu\text{m}$ . In the next step, the synthesized precursor particles were further annealed in  $\text{O}_2$  gas for 12 h at 800  $^{\circ}\text{C}$ , whereby the material crystallinity was improved and the layered-structure crystal phase was formed. In this step, single-crystal primary structures with sizes of 200–600 nm appeared and porous, irregularly shaped particles were formed. The original spherical shape from step 1 was completely changed during sintering in  $\text{O}_2$  gas at high temperature. The particle size and morphology have not been optimized since the objective of this study was proof-of-concept. Current agglomerated structures could be improved by changing atomizer conditions to produce larger droplets and therefore larger particles.

The material crystal structures were examined by XRD, and the results are compared in Figure 3. A simulated NCM811 ( $R\bar{3}m$ ) diffraction pattern (Figure 3(A)) was modelled by using the Visualization for Electronic and Structural Analysis (VESTA) program and compared with the XRD results of other crystal structures (Figure 3A) was modeled by using the visualization for electronic and structural analysis (VESTA) program and compared with the XRD results of other crystal structures (Figure 3B–D). The diffraction patterns indicate that the crystal structures of the pristine (undoped) and the Ca-doped NCM811 samples are consistent with a layered hexagonal structure.<sup>20</sup> The layered structure of all three samples was confirmed by the splitting of the (003)/(104), (006)/(012), and (018)/(110) peaks. This comparison further suggests the existence of cation mixing, as indicated by the decrease of the (003) and (104) peak ratio (1.21 for the ideal

NCM 811 model, 1.17 for pristine NCM811, 1.14 for uniform Ca-doped material, and 1.08 for gradient structure Ca-doped material). Murali et al. have observed a similar behavior in doping studies, indicating successful outcomes.<sup>29</sup>  $\text{Ca}^{2+}$  can be doped into the Li layer only since  $\text{Ca}^{2+}$  does not have the octahedral coordination needed in the transition metal (TM) layer. The doped  $\text{Ca}^{2+}$  in the Li layer could act as pillars to support the layered structure during the charge–discharge process.<sup>30,31</sup> A CaO phase was observed in gradient Ca-doped NCM811 materials (indicated as starred peaks) as shown in Figure 3D. The benefit of CaO will be discussed later. In brief, the strong Ca–O bonds inhibit surface reactions with electrolytes, which increases the thermal stability of the cathode material.

The elemental compositions of the particles were analyzed by using EDX, and the results are compared in Figure 4, indicating that the Ni, Co, Mn, and Ca elemental compositions were conserved in the synthesis process when compared with those in the precursor solutions. The EDX mapping results (Figure 4, right) show the distribution of each element in both gradient and uniform Ca-doped NCM811 particles. A uniform distribution of all elements was observed in all the uniform Ca-doped NCM811 particles, without detection of any Ca-rich phases.

The surface and deeper elemental compositions were analyzed by using XPS on both the uniform Ca-doped and gradient Ca-doped particles. The Ca 2p<sub>3/2</sub> peak in XPS at 347.3 eV binding energy (BE) (Figure 5, left) shows the presence of Ca on the surface and at 120 nm depth. Specifically, this peak could only be of CaO as  $\text{CaCO}_3$  is not part of the synthesis process.<sup>32,33</sup> As shown in Figure 5 left, the

Ca concentration on the surface is about 10 times higher than the concentration at 120 nm depth, which is strong evidence of the gradient structure. Depth profiles (Figure 5, right) show that the Ca/Ni atomic ratio decreases with increasing depth from the surface in the gradient structure material, while the uniform structure material has a relatively constant Ca/Ni ratio throughout the material. This confirms that precursor chemical control in aerosol synthesis enables the product powders to retain the concentration gradient structure even after annealing; such a structure is hypothesized to be favorable for reducing parasitic reactions between the cathode and the electrolyte. A key mechanism to form a gradient structure is the difference in solubility of the precursors in solution. During the heating process, calcium sulfate in the precursor precipitates on the surface before the other metal salts, thus forming the gradient structure, while calcium nitrate causes Ca precipitation to occur simultaneously with the other metal elements.

Electrochemical analysis was performed using coin cells with graphite anodes and these synthesized materials as cathodes. The comparison between pristine NCM811, 1.5% uniform Ca-doped NCM811, and 1.5% gradient Ca-doped NCM811 is shown in Figure 6. All materials had a stable and smooth

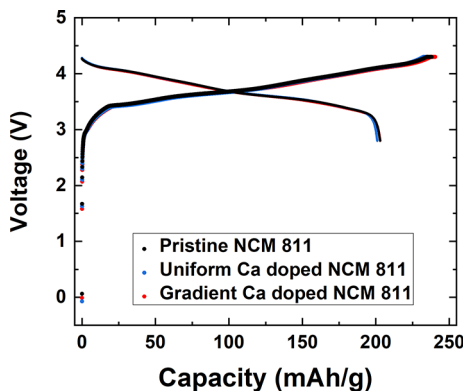


**Figure 6.** Initial charge/discharge curves of pristine and Ca-doped NCM811 cells.

charge–discharge behavior without obvious polarization. Pristine NCM811 initially exhibited a discharge capacity of  $201 \text{ mA h g}^{-1}$ , while the initial discharge capacity for Ca-doped electrodes in the first cycle was  $198 \text{ mA h g}^{-1}$  for uniform Ca doping and  $196 \text{ mA h g}^{-1}$  for gradient Ca doping. The marginally lower capacity for the gradient Ca-doped material is due to the redox-inactive Ca doping. All materials had regular charge–discharge curves, further confirming dopant incorporation without any significant change in the material phase or chemistry, which also enabled a significantly improved thermal stability.

Thermal stability is one of the biggest challenges for the commercialization of NCM811. The delithiated cathode materials of pristine NCM811, uniform Ca-doped NCM811, and gradient Ca-doped NCM811 were compared in thermal decomposition testing after charging at 0.1C to a delithiated state. Delithiated cathode materials were heated in a tubular micro-flow reactor, and the gaseous products were monitored using a mass spectrometer. The decomposition and material stability properties were analyzed based on the gaseous products. Pristine NCM811 starts releasing  $\text{O}_2$  at 494 K, which ends at 673 K as shown in Figure 7. This temperature

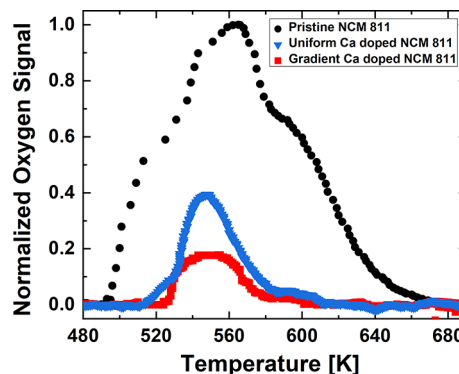


**Figure 7.** Thermal decomposition profile of delithiated pristine NCM811 (black), uniform Ca-doped NCM 811 (blue) and gradient Ca-doped NCM811 (red).

region represents the material decomposition process. Uniform Ca-doped material showed a higher decomposition temperature at 515 K and a shorter decomposition range (515 K–612 K) that indicates thermal stabilization with Ca doping. In addition, gradient Ca-doped material starts to decompose at an even higher temperature of 527 K, which ends at 583 K. As mentioned above, the higher concentration of Ca on the material surface in the gradient structure provides better protection and stabilizes the surface compared to that in uniform Ca doping. Such a Ca-rich layer helps maintain the structural stability during the decomposition process and provides a protective barrier for the cathode material. XRD results indicate that the gradient structure material has an additional CaO phase that might provide an additional physical barrier between the cathode materials and residual electrolyte.

Beyond the decomposition temperature delay, Ca doping also helps reduce the amount of oxygen released for the cathode material. Oxygen release is a key factor in cathode decomposition that dominates the heat release in such a process.<sup>17,34</sup> When the areas under the oxygen release profile were compared, the uniform Ca-doped NCM811 showed a 52% improvement (decrease) in the oxygen release and gradient Ca-doped NCM811 showed an 85% improvement in oxygen release compared to that of pristine NCM811. Visually, compared to pristine NCM811, Ca-doped materials produced more solid decomposition residual material after decomposition tests. A detailed explanation still requires further investigation, but one possible reason is that Ca doping stabilizes the cathode material during heating. The Ni cations are present as high-valence  $\text{Ni}^{4+}$  after charging, but during the thermal decomposition process,  $\text{Ni}^{4+}$  is reduced to a lower valence  $\text{Ni}^{2+}$  and releases oxygen.<sup>10</sup> Ca doping localizes lattice oxygen and decelerates the reduction process and changes the reaction pathway to produce more solid products. In summary, this Ca doping technique strongly stabilizes NCM811 by minor cation mixing of Ni and Ca and suppresses oxygen release during the thermal decomposition process in the material, which results in better thermal stability. More specifically, gradient Ca doping reduces the release of  $\text{O}_2$  gas even further, which is of great significance in improving the thermal stability and creating better fire-resistant LIBs.

#### 4. CONCLUSIONS

In this study, we successfully incorporated uniform and concentration-gradient Ca dopants in NCM811 cathode materials by using a high-temperature aerosol synthesis

method with subsequent heat treatment. We showed that the Ca precursor can be used to tailor the dopant distribution within the cathode particle. The Ca doping strongly stabilized the crystal structure of NCM811, resulting in enhanced thermal stability. In thermal decomposition tests of the delithiated materials, both Ca-doped NCM811 materials showed superior fire safety with significantly less oxygen release and increased thermal decomposition temperature. The gradient structure material is superior to the uniformly doped material because Ca doping localizes lattice oxygen that decelerates the reduction process, particularly at the reactive cathode–electrolyte interface and changes the reaction pathway to produce more solid products. Ca doping stabilizes the cathode particle surface as well as the bulk layered structure. The doped materials exhibited a good first cycle discharge capacity of close to  $200 \text{ mA h g}^{-1}$ . In summary, rapid ( $\sim 10 \text{ s}$ ) formation of a concentration gradient structure in aerosol synthesis is a promising route in optimizing the thermal stability of cathode materials for LIBs and is a novel route for local control of doping in electrode materials.

## ASSOCIATED CONTENT

### Supporting Information

The Supporting Information is available free of charge at <https://pubs.acs.org/doi/10.1021/acsaem.2c01471>.

Coin cell electrochemical analysis and differential capacity analysis (PDF)

## AUTHOR INFORMATION

### Corresponding Author

**Chao Yan** — Department of Mechanical and Aerospace Engineering, Princeton University, Princeton, New Jersey 08544, United States;  [orcid.org/0000-0002-2415-6080](https://orcid.org/0000-0002-2415-6080); Email: [chaoy@princeton.edu](mailto:chaoy@princeton.edu)

### Authors

**Ying Lin** — Department of Mechanical and Aerospace Engineering, Princeton University, Princeton, New Jersey 08544, United States;  [orcid.org/0000-0002-1148-152X](https://orcid.org/0000-0002-1148-152X)

**Christopher M. Abram** — Department of Mechanical and Aerospace Engineering, Princeton University, Princeton, New Jersey 08544, United States; HiT Nano, Inc., Bordentown, New Jersey 08505, United States

**Xuan Shi** — Department of Mechanical and Aerospace Engineering, Princeton University, Princeton, New Jersey 08544, United States; HiT Nano, Inc., Bordentown, New Jersey 08505, United States

**Ian G. McKendry** — HiT Nano, Inc., Bordentown, New Jersey 08505, United States

**Ziyu Wang** — Department of Mechanical and Aerospace Engineering, Princeton University, Princeton, New Jersey 08544, United States;  [orcid.org/0000-0003-2914-6460](https://orcid.org/0000-0003-2914-6460)

**Hongtao Zhong** — Department of Mechanical and Aerospace Engineering, Princeton University, Princeton, New Jersey 08544, United States

**Hao Zhao** — Department of Mechanical and Aerospace Engineering, Princeton University, Princeton, New Jersey 08544, United States

**Xiaofang Yang** — Princeton NuEnergy, Inc., Bordentown, New Jersey 08505, United States

**Bruce E. Koel** — Department of Chemical and Biological Engineering, Princeton University, Princeton, New Jersey 08544, United States;  [orcid.org/0000-0002-0032-4991](https://orcid.org/0000-0002-0032-4991)

**Yiguang Ju** — Department of Mechanical and Aerospace Engineering, Princeton University, Princeton, New Jersey 08544, United States

Complete contact information is available at:  
<https://pubs.acs.org/10.1021/acsaem.2c01471>

### Author Contributions

The manuscript was written through contributions of all authors. All authors have given approval to the final version of the manuscript.

### Funding

HiT Nano acknowledge partial support of DOE SBIR/STTR contract DE-SC0019893 and BIRD Energy project 7131. Co-authors B.E.K and C.Y. acknowledge partial support for this research by Princeton University under the Princeton IP Accelerator Fund.

### Notes

The authors declare no competing financial interest.

## REFERENCES

- (1) Goodenough, J. B. How we made the Li-ion rechargeable battery. *Nat. Electron.* **2018**, *1*, 204.
- (2) Ding, Y.; Cano, Z. P.; Yu, A.; Lu, J.; Chen, Z. Automotive Li-ion batteries: current status and future perspectives. *Electrochim. Energy Rev.* **2019**, *2*, 1–28.
- (3) Choi, J. W.; Aurbach, D. Promise and reality of post-lithium-ion batteries with high energy densities. *Nat. Rev. Mater.* **2016**, *1*, 1–16.
- (4) Xu, X.; Huo, H.; Jian, J.; Wang, L.; Zhu, H.; Xu, S.; He, X.; Yin, G.; Du, C.; Sun, X. Radially Oriented Single-Crystal Primary Nanosheets Enable Ultrahigh Rate and Cycling Properties of  $\text{LiNi}_{0.8}\text{Co}_{0.1}\text{Mn}_{0.1}\text{O}_2$  Cathode Material for Lithium-Ion Batteries. *Adv. Energy Mater.* **2019**, *9*, 1803963.
- (5) Park, J. H.; Choi, B.; Kang, Y. S.; Park, S. Y.; Yun, D. J.; Park, I.; Shim, J. H.; Park, J. H.; Han, H. N.; Park, K. Effect of Residual Lithium Rearrangement on Ni-rich Layered Oxide Cathodes for Lithium-Ion Batteries. *Energy Technol.* **2018**, *6*, 1361–1369.
- (6) Ryu, H. H.; Park, G. T.; Yoon, C. S.; Sun, Y. K. Microstructural Degradation of Ni-Rich Li  $[\text{Ni}_x\text{Co}_y\text{Mn}_{1-x-y}]_{\text{O}_2}$  Cathodes During Accelerated Calendar Aging. *Small* **2018**, *14*, 1803179.
- (7) Kim, J.; Lee, H.; Cha, H.; Yoon, M.; Park, M.; Cho, J. Prospect and Reality of Ni-Rich Cathode for Commercialization. *Adv. Energy Mater.* **2018**, *8*, 1702028.
- (8) Liu, K.; Liu, Y.; Lin, D.; Pei, A.; Cui, Y. Materials for lithium-ion battery safety. *Sci. Adv.* **2018**, *4*, No. eaas9820.
- (9) Wang, Q.; Ping, P.; Zhao, X.; Chu, G.; Sun, J.; Chen, C. Thermal runaway caused fire and explosion of lithium ion battery. *J. Power Sources* **2012**, *208*, 210–224.
- (10) Bak, S.-M.; Hu, E.; Zhou, Y.; Yu, X.; Senanayake, S. D.; Cho, S.-J.; Kim, K.-B.; Chung, K. Y.; Yang, X.-Q.; Nam, K.-W. Structural changes and thermal stability of charged  $\text{LiNi}_x\text{Mn}_y\text{Co}_z\text{O}_2$  cathode materials studied by combined in situ time-resolved XRD and mass spectroscopy. *ACS Appl. Mater. Interfaces* **2014**, *6*, 22594–22601.
- (11) Yan, W.; Yang, S.; Huang, Y.; Yang, Y.; Guohui Yuan, G. A review on doping/coating of nickel-rich cathode materials for lithium-ion batteries. *J. Alloys Compd.* **2020**, *819*, 153048.
- (12) Li, Y.-C.; Xiang, W.; Wu, Z.-G.; Xu, C.-L.; Xu, Y.-D.; Xiao, Y.; Yang, Z.-G.; Wu, C.-J.; Lv, G.-P.; Guo, X.-D. Construction of homogeneously  $\text{Al}^{3+}$  doped Ni rich Ni-Co-Mn cathode with high stable cycling performance and storage stability via scalable continuous precipitation. *Electrochim. Acta* **2018**, *291*, 84–94.
- (13) Schipper, F.; Bouzaglo, H.; Dixit, M.; Erickson, E. M.; Weigel, T.; Talianker, M.; Grinblat, J.; Burstein, L.; Schmidt, M.; Lampert, J.; Erk, C.; Markovsky, B.; Major, D. T.; Aurbach, D. From surface  $\text{ZrO}_2$

- coating to bulk Zr doping by high temperature annealing of nickel-rich lithiated oxides and their enhanced electrochemical performance in lithium ion batteries. *Adv. Energy Mater.* **2018**, *8*, 1701682.
- (14) Manthiram, A.; Song, B.; Li, W. A perspective on nickel-rich layered oxide cathodes for lithium-ion batteries. *Energy Storage Mater.* **2017**, *6*, 125–139.
- (15) Chen, Z.; Qin, Y.; Amine, K.; Sun, Y.-K. Role of surface coating on cathode materials for lithium-ion batteries. *J. Mater. Chem.* **2010**, *20*, 7606–7612.
- (16) Myung, S.-T.; Amine, K.; Sun, Y.-K. Surface modification of cathode materials from nano-to microscale for rechargeable lithium-ion batteries. *J. Mater. Chem.* **2010**, *20*, 7074–7095.
- (17) Cho, J.; Kim, T.-G.; Kim, C.; Lee, J.-G.; Kim, Y.-W.; Park, B. Comparison of  $\text{Al}_2\text{O}_3$ -and  $\text{AlPO}_4$ -coated  $\text{LiCoO}_2$  cathode materials for a Li-ion cell. *J. Power Sources* **2005**, *146*, 58–64.
- (18) Kalluri, S.; Yoon, M.; Jo, M.; Liu, H. K.; Dou, S. X.; Cho, J.; Guo, Z. Feasibility of cathode surface coating technology for high-energy lithium-ion and beyond-lithium-ion batteries. *Adv. Mater.* **2017**, *29*, 1605807.
- (19) Wang, Y.-Y.; Gao, M.-Y.; Liu, S.; Li, G.-R.; Gao, X.-P. Yttrium surface gradient doping for enhancing structure and thermal stability of high-Ni layered oxide as cathode for Li-ion batteries. *ACS Appl. Mater. Interfaces* **2021**, *13*, 7343–7354.
- (20) Chen, M.; Zhao, E.; Chen, D.; Wu, M.; Han, S.; Huang, Q.; Yang, L.; Xiao, X.; Hu, Z. Decreasing Li/Ni disorder and improving the electrochemical performances of Ni-rich  $\text{LiNi}_{0.8}\text{Co}_{0.1}\text{Mn}_{0.1}\text{O}_2$  by Ca doping. *Inorg. Chem.* **2017**, *56*, 8355–8362.
- (21) Ding, Y.; Zhang, P.; Jiang, Y.; Gao, D. Effect of rare earth elements doping on structure and electrochemical properties of  $\text{LiNi}_{1/3}\text{Co}_{1/3}\text{Mn}_{1/3}\text{O}_2$  for lithium-ion battery. *Solid State Ionics* **2007**, *178*, 967–971.
- (22) Schougaard, S. B.; Bréger, J.; Jiang, M.; Grey, C. P.; Goodenough, J. B.  $\text{LiNi}_{0.5+\delta}\text{Mn}_{0.5-\delta}\text{O}_2$ —A High-Rate, High-Capacity Cathode for Lithium Rechargeable Batteries. *Adv. Mater.* **2006**, *18*, 905–909.
- (23) Zhao, E.; Hu, Z.; Xie, L.; Chen, X.; Xiao, X.; Liu, X. A study of the structure–activity relationship of the electrochemical performance and Li/Ni mixing of lithium-rich materials by neutron diffraction. *RSC Adv.* **2015**, *5*, 31238–31244.
- (24) Wu, E. J.; Telesh, P. D.; Ceder, G. Size and charge effects on the structural stability of  $\text{LiMO}_2$  ( $M =$  transition metal) compounds. *Philos. Mag. B* **1998**, *77*, 1039–1047.
- (25) Wang, L.; Maxisch, T.; Ceder, G. A first-principles approach to studying the thermal stability of oxide cathode materials. *Chem. Mater.* **2007**, *19*, 543–552.
- (26) Dahn, J.; Fuller, E.; Obrovac, M.; Von Sacken, U. Thermal stability of  $\text{Li}_x\text{CoO}_2$ ,  $\text{Li}_x\text{NiO}_2$  and  $\lambda\text{-MnO}_2$  and consequences for the safety of Li-ion cells. *Solid State Ionics* **1994**, *69*, 265–270.
- (27) Abram, C.; Shan, J.; Yang, X.; Yan, C.; Steingart, D.; Ju, Y. Flame Aerosol Synthesis and Electrochemical Characterization of Ni-Rich Layered Cathode Materials for Li-Ion Batteries. *ACS Appl. Energy Mater.* **2019**, *2*, 1319–1329.
- (28) Yan, C.; Yang, X.; Zhao, H.; Zhong, H.; Ma, G.; Qi, Y.; Koel, B. E.; Ju, Y. Controlled Dy-doping to nickel-rich cathode materials in high temperature aerosol synthesis. *Proc. Combust. Inst.* **2021**, *38*, 6623–6630.
- (29) Murali, N.; Margarete, S.; Veeriah, V. Synthesis, dielectric, conductivity and magnetic studies of  $\text{LiNi}_{1/3}\text{Co}_{1/3}\text{Mn}_{(1/3)-x}\text{Al}_x\text{O}_2$  ( $x = 0.0, 0.02, 0.04$  and  $0.06$ ) for cathode materials of lithium-ion batteries. *Results Phys.* **2017**, *7*, 1379–1388.
- (30) Laisa, C.; Ramesha, R.; Ramesha, K. Enhanced electrochemical performance of lithium rich layered cathode materials by  $\text{Ca}^{2+}$  substitution. *Electrochim. Acta* **2017**, *256*, 10–18.
- (31) Uygur, C. S.; Aydinol, M. K. Effect of calcium or yttrium doping on cation ordering and electrochemical performance of  $\text{Li}(\text{Ni}_{0.80-x}\text{Co}_{0.15}\text{Al}_{0.05}\text{M}_x)\text{O}_2$  ( $M = \text{Ca}, \text{Y}$ ) as a Li-ion battery cathode. *Mater. Sci. Eng., B* **2021**, *264*, 114925.
- (32) Hanawa, T. Titanium and its oxide film: a substrate for formation of apatite. *The Bone-Biomaterial Interface*; University of Toronto Press, 1991.
- (33) Demri, B.; Muster, D. XPS study of some calcium compounds. *J. Mater. Process. Technol.* **1995**, *55*, 311–314.
- (34) Arai, H.; Tsuda, M.; Saito, K.; Hayashi, M.; Sakurai, Y. Thermal reactions between delithiated lithium nickelate and electrolyte solutions. *J. Electrochem. Soc.* **2002**, *149*, A401.

## □ Recommended by ACS

### **Li<sub>0.9</sub>Co<sub>0.09</sub>Mo<sub>0.01</sub>O<sub>2</sub> Cathode with Li<sub>3</sub>PO<sub>4</sub> Coating and Ti Doping for Next-Generation Lithium-Ion Batteries**

Yongjiang Sun, Hong Guo, *et al.*

FEBRUARY 28, 2023

ACS ENERGY LETTERS

READ ▶

### **Ta Doping Improves the Cyclability and Rate Performance of a Nickel-Rich NCA Cathode via Promoted Electronic and Cationic Conductivity**

Yanyan Liu, Chengkang Chang, *et al.*

NOVEMBER 28, 2022

ACS SUSTAINABLE CHEMISTRY & ENGINEERING

READ ▶

### **Double Conductor Coating to Improve the Structural Stability and Electrochemical Performance of Li<sub>0.8</sub>Co<sub>0.1</sub>Mn<sub>0.1</sub>O<sub>2</sub> Cathode Material**

Yang Zhang, Jie Liu, *et al.*

JANUARY 31, 2023

ACS SUSTAINABLE CHEMISTRY & ENGINEERING

READ ▶

### **Sr-Based Sub/Surface Integrated Layer and Bulk Doping to Enhance High-Voltage Cycling of a Ni-Rich Cathode Material**

Longchao Wang, Qingyu Li, *et al.*

JUNE 10, 2022

ACS SUSTAINABLE CHEMISTRY & ENGINEERING

READ ▶

**Get More Suggestions >**